Available online at www.sciencedirect.com
SCIENCE DIRECT®
Combustion and Flame 142 (2005) 62–71
Combustion and Flame
www.elsevier.com/locate/combustflame

Scalar dissipation rate at extinction and the effects of oxygen-enriched combustion

R. Chen, R.L. Axelbaum *

Department of Mechanical Engineering, Washington University, St. Louis, MO 63130, USA

Received 25 August 2004; received in revised form 20 January 2005; accepted 1 February 2005
Available online 23 March 2005

Abstract

The strain rate at extinction was measured in the counterflow flame configuration for methane, propane, and ethane flames as a function of stoichiometric mixture fraction. To complement this, the scalar dissipation rate and flame temperature at extinction were evaluated numerically for methane, ethane, and ethylene flames. The stoichiometric mixture fraction, Z_{st}, was varied by removing nitrogen from the air (oxygen-enriched air) and introducing it to the fuel (diluted fuel) in such a way that the adiabatic flame temperature was not varied. In this way the effect of flame structure, as dictated by changes in stoichiometric mixture fraction, could be studied. The results indicate that the scalar dissipation rate at extinction is strongly affected by Z_{st}, and can be 15 to 40 times greater than that for neat fuel burning in air. The maximum does not occur at the highest Z_{st} (diluted fuel in oxygen) but rather between Z_{st} of 0.5 to 0.65 for the fuels considered. In addition, the flame temperature at extinction is affected by Z_{st} and reaches a minimum at nearly the same value of Z_{st} where the extinction scalar dissipation rate reaches a maximum. The numerical results indicate that at this Z_{st} the location of peak temperature is nearly coincident with the location of peak radical production. In the normal fuel/air flame the radical production zone is located on the oxidizer side of peak temperature in a location where the temperature is over 100 °C cooler. By shifting this zone to be coincident with the peak temperature the flame is stronger and more resistant to extinction, resulting in a greater scalar dissipation rate and a lower extinction temperature.

Keywords: Chemical structure; Oxygen-enriched combustion; Diffusion flames; Extinction; Laminar flames; Limits; Fuel dilution

1. Introduction

Oxygen-enriched combustion has been gaining greater acceptance in recent years. The potential value in terms of improved heat transfer [1] and reductions in soot [2] and NO_x [1] can offset the cost penalty of burning a fuel in an oxidizer other than air. Furthermore, the cost of oxygen is coming down and recently the DOE has proposed oxygen-enriched combustion with carbon sequestration as a means of reducing greenhouse gases [3]. Stack emissions of NO_x generally increase with flame temperature; thus, when nitrogen is removed from the air it is replaced with exhaust gases to keep the flame temperature sufficiently low.

Studies have shown that changes in oxygen and fuel concentration can have a dramatic effect on flame

* Corresponding author. Fax: +1 314 935 4014.
E-mail address: rla@wustl.edu (R.L. Axelbaum).

0010-2180/$ – see front matter
doi:10.1016/j.combustflame.2005.02.008

structure and consequently soot formation even when the temperature of the flame is kept constant [4]. Furthermore, the strain rate at extinction for methane has been shown to be enhanced with oxygen enrichment and fuel dilution [4]. In this paper we expand on this work to consider other fuels and to obtain a deeper understanding of the phenomena that is responsible for this behavior.

Studies of strained laminar opposed-flow diffusion flames have been extensively applied to develop a fundamental understanding of flame structure and extinction [5–7]. At a fixed nozzle separation distance, increasing the opposed-jet exit velocities increases gradients of axial velocity (strain rate) and the gradients of fuel and oxidizer concentration in the mixing layer, hence decreasing the local diffusion time in the vicinity of the flame. Since the characteristic chemical reaction time does not change, the second Damköhler number Da—defined as the ratio of the diffusion time to the chemical reaction time—will also decrease. This decrease subjects the flame to nonequilibrium effects and eventually results in stretch-induced extinction [8]. When these effects are important, the fast chemistry assumption fails and the scalar dissipation rate, which is the characteristic nonequilibrium parameter, must be taken into account. The scalar dissipation rate, χ, is defined by

$$\chi = 2D\left(\frac{\partial Z}{\partial x_\alpha}\right)^2 = 2D\left[\left(\frac{\partial Z}{\partial x_1}\right)^2 + \left(\frac{\partial Z}{\partial x_2}\right)^2 + \left(\frac{\partial Z}{\partial x_3}\right)^2\right]. \quad (1)$$

Here D is the diffusion coefficient and Z is the mixture fraction, which is the mass fraction of material that originated from the fuel stream and is given by

$$Z = \frac{Y_\mathrm{F}/W_\mathrm{F}\nu_\mathrm{F} + (Y_{\mathrm{O},-\infty} - Y_\mathrm{O})/W_\mathrm{O}\nu_\mathrm{O}}{Y_{\mathrm{F},\infty}/W_\mathrm{F}\nu_\mathrm{F} + Y_{\mathrm{O},-\infty}/W_\mathrm{O}\nu_\mathrm{O}}, \quad (2)$$

where Y is the mass fraction, W is the molecular weight, ν is the stoichiometric coefficient, and the subscripts F and O refer to fuel and oxidizer, respectively. The outer flame structure is characterized by the mixture fraction at the location of stoichiometry which is given by [9]

$$Z_\mathrm{st} = (1 + Y_{\mathrm{F},\infty}W_\mathrm{O}\nu_\mathrm{O}/Y_{\mathrm{O},-\infty}W_\mathrm{F}\nu_\mathrm{F})^{-1}. \quad (3)$$

The stoichiometric mixture fraction, Z_st, is a fundamental parameter that, along with adiabatic flame temperature, accounts for how oxygen enrichment and fuel dilution affect the global flame structure and for this reason we will use Z_st and adiabatic flame temperature to interpret the results.

The scalar dissipation rate at stoichiometric conditions χ_st represents the extent of heat conduction and species diffusion at the flame [10]. The flame structure consists essentially of a thin inner reaction zone embedded between two chemically inert outer zones. When χ_st is increased, heat conduction from, and reactant diffusion to, the reaction zone will increase. If this increase is beyond a critical value, χ_q, incomplete reaction results in reactant leakage and thus heat conduction can no longer be balanced by heat production due to chemical reaction, and the flame is extinguished. This behavior results in the well-known S-shaped curve. Basically, extinction occurs when the characteristic time of flow of reactants through the reaction zone becomes shorter than the time required for heat release through chemical reaction. As the second Damköhler number Da is reduced to a critical value Da_Q, extinction occurs.

The Da is inversely proportional to χ_st provided that the characteristic chemical reaction time does not change. The critical value χ_q is the condition where finite rate kinetics just balances diffusion and corresponds to Da_Q. As such, it can be recognized as an indicator of flame strength.

In this work we will study the effects of flame structure on extinction limits in counterflow diffusion flames for a variety of fuels when the oxidizer is enriched and the fuel is diluted, i.e., when the stoichiometric mixture fraction is increased. To this end, the strain rate at extinction is measured in the counterflow flame configuration for methane, propane, and ethane flames as a function of stoichiometric mixture fraction. To compliment this, the scalar dissipation rate and flame temperature at extinction are evaluated numerically for methane, ethane, and ethylene flames. The stoichiometric mixture fraction, Z_st, is varied by removing nitrogen from the air (oxygen-enriched air) and introducing it to the fuel (diluted fuel) in such a way that the adiabatic flame temperature is not varied. In this way the effect of flame structure, as dictated by changes in stoichiometric mixture fraction, can be studied.

2. Experimental and numerical methodology

The experimental apparatus is described in detail in Du and Axelbaum [9]. Briefly, a flame is established between two 11-mm opposed jets spaced 6 mm apart. The jets emanate from tubes with honeycomb cores placed 50 cm upstream of each exit. The complete flow field has not been characterized, but the far field is expected to behave between potential and plug flow [8]. An annular coflow of nitrogen is added to both fuel and oxidizer to eliminate oxygen entrainment from ambient air and to extinguish the flame that would exist outside the region of interest.

Table 1
Flames considered in the numerical and experimental work

	CH_4, $T_{ad} = 2226$ K			C_2H_4, $T_{ad} = 2370$ K			C_2H_6, $T_{ad} = 2260$ K			C_3H_8, $T_{ad} = 2267$ K		
	Z_{st}	Y_{CH_4} at $Z = 1$	Y_{O_2} at $Z = 0$	Z_{st}	$Y_{C_2H_4}$ at $Z = 1$	Y_{O_2} at $Z = 0$	Z_{st}	$Y_{C_2H_6}$ at $Z = 1$	Y_{O_2} at $Z = 0$	Z_{st}	$Y_{C_3H_8}$ at $Z = 1$	Y_{O_2} at $Z = 0$
Flame A	0.055	1.0	0.233	0.064	1.0	0.233	0.059	1.0	0.233	0.060	1.0	0.233
Flame B	0.35	0.157	0.339	0.35	0.182	0.336	0.35	0.167	0.338	0.35	0.172	0.337
Flame C	0.5	0.111	0.437	0.5	0.127	0.437	0.5	0.118	0.439	0.5	0.121	0.438
Flame D	0.65	0.085	0.632	0.65	0.098	0.624	0.65	0.090	0.627	0.65	0.093	0.626
Flame E	0.78	0.071	1.0	0.78	0.081	1.0	0.78	0.075	1.0	0.78	0.077	1.0

To obtain extinction strain rates, the flow rate is increased until extinction occurs. A bypass is used to ensure that the composition remains fixed as strain rate is increased. The flame is then reestablished at conditions very near extinction, and the velocity profile along the stagnation streamline is measured with laser-Doppler velocimetry. The strain rate, K, is identified as the magnitude of the slope of the velocity profile upstream of the flame. Because the densities of the fuel and the oxidizer free streams are similar, the velocity gradients on both sides of the flame are identical within experimental uncertainties.

The numerical scheme employed was the counterflow code developed by Smooke et al. [11]. The version of the code used here can model both potential and plug-flow boundary conditions at the edge of the boundary layer [12]. The strain rate K was obtained as in [2]. The reaction mechanism is a 202-step reduced GRI mechanism based on GRI 3.0 [13] in which all nitrogen species except N_2, N, and NO are deleted. Before eliminating the trace nitrogen species we carefully compared results from the original and the reduced mechanism and found no significant difference in our test cases. This is as expected since the species eliminated, while important to NO formation, are not important to the bulk flame chemistry.

3. Results and discussion

As described in detail in Du and Axelbaum [2,9], in order to isolate the effects of flame structure resulting from shifts in flame location, the stoichiometric mixture fraction must be changed without changing the adiabatic flame temperature. This is accomplished by keeping a fixed amount of the inert component (nitrogen in this work) at the flame while varying the relative amount that is added to the fuel and oxidizer. Experimentally, for a fuel with stoichiometry given by

$$C_nH_m + (n + m/4)O_2 + 3.76(n + m/4)N_2 \rightarrow \text{products} \quad (4)$$

this is accomplished by choosing flow rates that satisfy

$$Q_{N_2,O}/Q_O + Q_{N_2,F}/(n + m/4)Q_F = 3.76, \quad (5)$$

where $Q_{N_2,i}$ is the flow rate of nitrogen mixed with the ith species, and subscripts O and F refer to O_2 and fuel, respectively. To obtain the widest range of Z_{st} and thus observe structural effects more clearly, flames are considered between and including the two extreme cases: where all the nitrogen is introduced with the oxidizer and where it is introduced with the fuel. Table 1 lists all flames that were considered in the numerical and experimental works.

In order to show that the effects of stoichiometric mixture fraction on extinction are similar for all fuels, several fuels were investigated: Methane, ethylene, and ethane were considered as fuels for the numerical work, while methane, ethane, and propane were used as fuels for the experimental work. Propane was not modeled because there are no well-accepted mechanisms for propane that have been validated for flame extinction and mechanism validation is not the focus of this work. Ethylene was not measured experimentally due to its extremely high extinction strain rate.

In Figs. 1 and 2, the extinction strain rates K_{ext} are plotted as functions of Z_{st}. From Fig. 1, for methane flames, the strain rate K_{ext} required to extinguish the diluted methane–oxygen flame is more than two times as high as that for the methane–air flame. As Z_{st} increases from 0.055 to 0.78, the experimentally measure K_{ext} increases from 370 to 898 s^{-1}. For a potential flow boundary condition the numerical results yield an increase from 393 to 883 s^{-1} and for plug flow it is from 223 to 468 s^{-1}. Results for other fuels are shown in Fig. 2. The extinction strain rates for the other fuels also show a trend where they increase with Z_{st} but the increase is less than that for CH_4 and the increase may not be monotonic for C_2H_6 and C_3H_8. The extinction strain rates K_{ext} for C_2H_4 flames are very high: the lowest is 2358 s^{-1}, as predicted numerically. This was beyond the capabilities of the experimental apparatus and, thus, K_{ext} was not measured experimentally for C_2H_4.

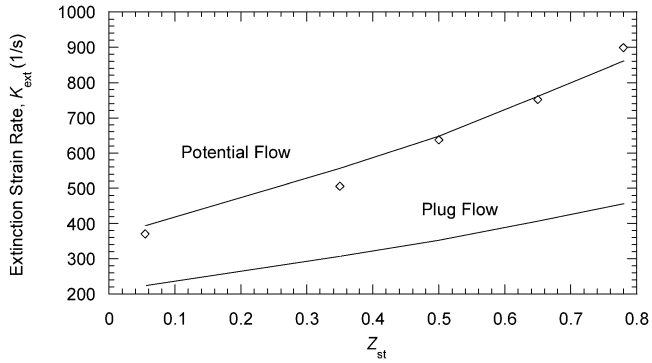

Fig. 1. Extinction strain rates as function of stoichiometric mixture fraction for CH_4 flames, all with the same adiabatic temperature. Symbols are experimental data and curves represent numerical results, using either the potential flow or the plug-flow assumptions.

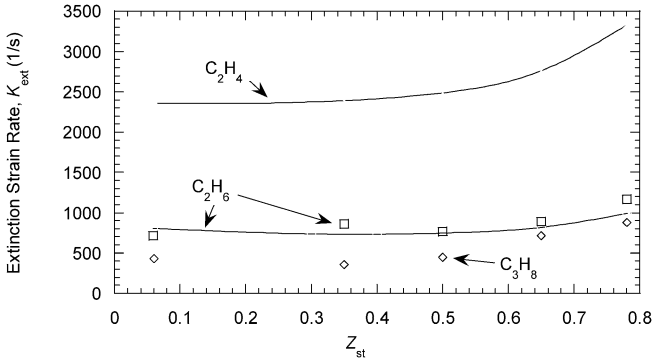

Fig. 2. Extinction strain rates as a function of stoichiometric mixture fraction for C_2H_4, C_2H_6, and C_3H_8 flames. Symbols are experimental data and curves represent numerical results assuming potential flow in the free stream.

In Fig. 1 numerical results for the two different free stream conditions—potential flow and plug flow—are compared with the experimental results for the methane flames. The experimental results are very close to the results reported in Ref. [4]. There is a significant difference in the extinction strain rate calculated assuming potential flow and plug flow, though both results show the trend of increasing K_{ext} with Z_{st}. The extinction strain rates computed using potential flow are about 2 times larger than those computed using plug flow. The potential flow results are very close to the experimental measurements, suggesting that the potential flow assumption is a good approximation of the flow field. This is reasonable for the experimental configuration used in this study because the jets in these experiments were produced from a tube, not a contracting nozzle and the separation distance of the jets was small. These conditions are expected to yield a flow field that is closer to potential flow than plug flow. For these reasons the potential flow assumption is applied to obtain the numerical results for the other fuels.

As stated earlier, the critical scalar dissipation rate can be recognized as an indicator of flame strength and thus the variation of χ_q with Z_{st} is investigated next. For a fixed diffusion coefficient, the critical scalar dissipation rate is characterized by the square of the gradient of mixture fraction at the flame location. In Fig. 3, mixture fractions are plotted as functions of arbitrary distance for the five flames near extinction. Plotting in terms of arbitrary distance allowed all five curves to be unambiguously plotted in the same figure without affecting the important quantity, which is the gradient of mixture fraction. The flame locations are also shown. Although the slope of the linear portion of the Z profile does steepen for higher strain rate, the increase is comparatively small. On the other hand, the location of the flame moves significantly, and this translates to a significant difference in the critical scalar dissipation rate, as indicated by the slope at the location of the flame.

In Figs. 4 and 5, the results for the extinction scalar dissipation rates χ_q (as characterized by $(dZ/dx)^2$ at Z_{st}) are plotted as functions of Z_{st}. The scalar

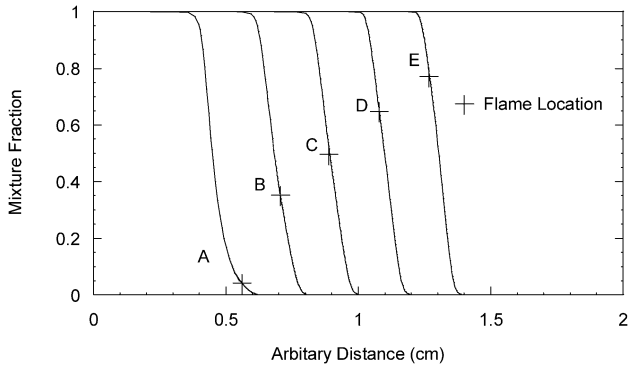

Fig. 3. Mixture fraction as function of distance for CH_4 flames assuming potential flow in the free stream. Flame location (location where $Z = Z_{st}$) is shown by a cross.

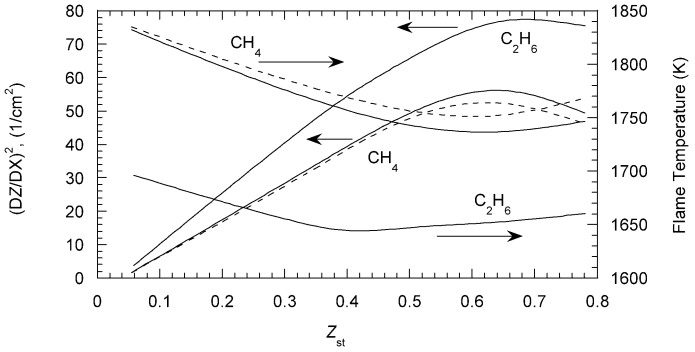

Fig. 4. Scalar dissipation rate and temperature near extinction as a function of Z_{st} for CH_4 and C_2H_6 flames. Solid lines are results for potential flow and dash lines for plug flow.

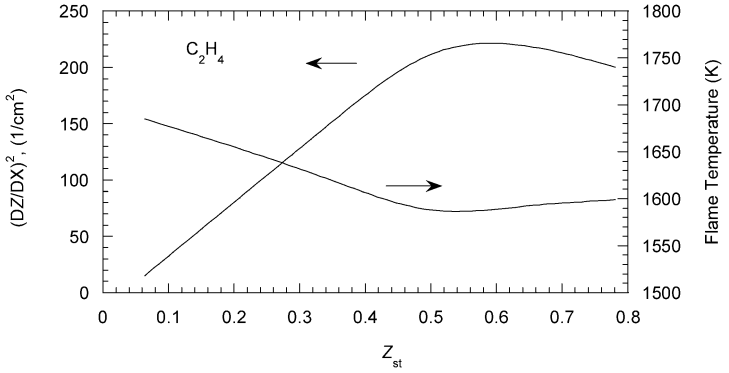

Fig. 5. Scalar dissipation rate and temperature near extinction as a function of Z_{st} for C_2H_4 flames using the potential flow assumption.

dissipation rate at extinction dramatically increases to a maximum value and then decreases with Z_{st} for all fuels. For CH_4, $(dZ/dx)^2$ varies from 1.6 to 56 cm^{-2}; for C_2H_4, from 15.1 to 216 cm^{-2}; and for C_2H_6, from 3.7 to 77 cm^{-2}. These increases suggest stronger flames, faster chemistry, and hence flames that are more difficult to extinguish. An important corollary to this is that for all fuels tested the value of Z_{st} that yields a maximum in χ_q corresponds to nearly the value that yields a minimum in extinction temperature, T_q. For CH_4, this occurs when Z_{st} is 0.65, and for C_2H_4 this occurs between 0.5 and 0.6. For C_2H_6, the correspondence between maximum χ_q and minimum T_q is not as strong, possibly due to the slow variation in T_q with Z_{st}. In other words, an uncertainty of only 10 °C in temperature would al-

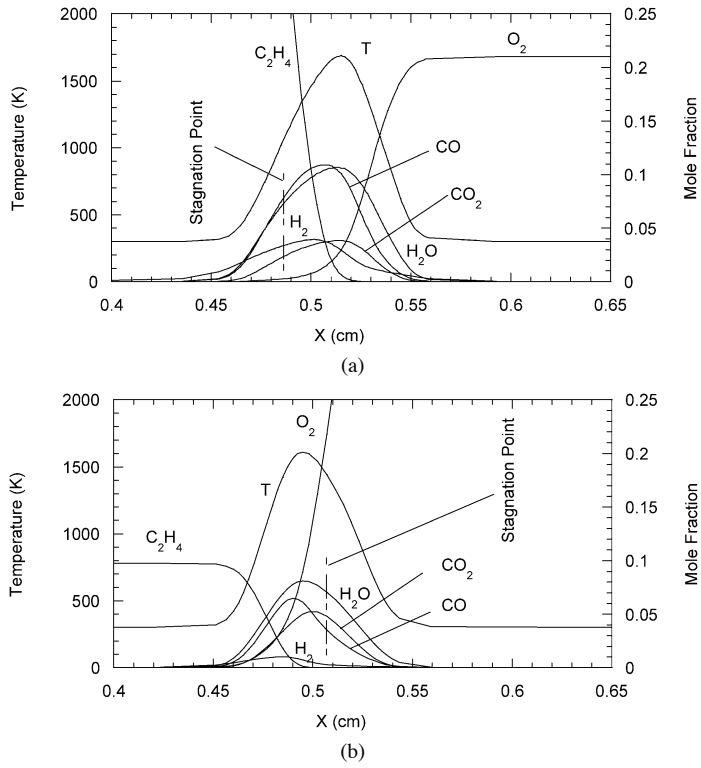

Fig. 6. Major species profiles and temperature near extinction for C_2H_4 flames: (a) fuel/air, $Z_{st} = 0.064$ and (b) diluted fuel/oxygen, $Z_{st} = 0.78$.

low the maximum χ_q to align with the minimum T_q. Assuming that the maximum in χ_q is accurate, this occurs around 0.6.

As discussed with regard to Fig. 1, there is a large difference between the potential flow and plug-flow solutions for the extinction strain rates for CH_4. Nonetheless, as shown in Fig. 4, the results are in good agreement when interpreted in terms of scalar dissipation rate χ_q. The temperatures are also similar. These results indicate that even though the flow fields are significantly different, the scalar dissipation rates at extinction are similar, and, accordingly, the extinction temperatures are similar. This agreement is anticipated because χ_q is a more direct measure of the limits of extinction than the extinction strain rate K_{ext}, particularly when Z_{st} is varied. The scalar dissipation rate at extinction is based on the conserved scalar Z and may be interpreted as the inverse of the characteristic diffusion time.

Since the adiabatic flame temperatures of flames A–E are identical, the primary effect of increasing Z_{st} is to shift the flame from the oxidizer toward the fuel, thereby changing the outer structure of the flame. Fig. 6 shows the profiles of temperature and major species for conditions near extinction for the C_2H_4 flames A and E. The location of the stagnation point is shown for reference. As Z_{st} increases, the flame moves toward the stagnation point and with sufficiently high Z_{st} it moves into the fuel side.

As Z_{st} increases, the relative amount of oxygen in the high temperature zone increases and the amount of fuel decreases. The increase in oxygen in the high temperature zone is beneficial for the stability of the flame because it will lead to faster generation of radicals by accelerating the chain-branching reaction

$$H + O_2 \rightarrow OH + O, \tag{6}$$

which provides greater resistance to extinction. Results show that for the same strain rate the high Z_{st} flames have a much greater radical pool than the low Z_{st} flames.

One might expect that since the amount of O_2 in the flame zone increases with Z_{st} this would lead to a monotonic increase in χ_q with Z_{st}. Such is not the case, as seen in Figs. 4 and 5. The reason for this can be understood with the aid of Figs. 7 and 8, where the rates of the dominant radical production reactions at extinction for flames A and D are plotted as functions of position for CH_4 and C_2H_4 flames, respectively. The stoichiometric mixture fraction is seen to affect the location of the radical production zone relative to that of the peak temperature. For flame A, the stan-

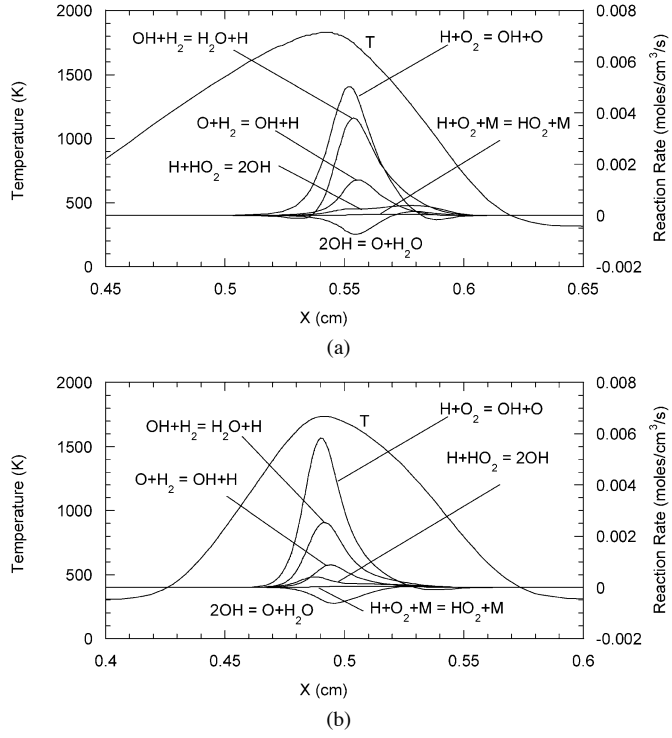

Fig. 7. Reaction rate profiles for the primary radical production reactions and temperature for CH_4 flames: (a) fuel/air, $Z_{st} = 0.055$ and (b) diluted fuel/oxygen-enriched air, $Z_{st} = 0.65$.

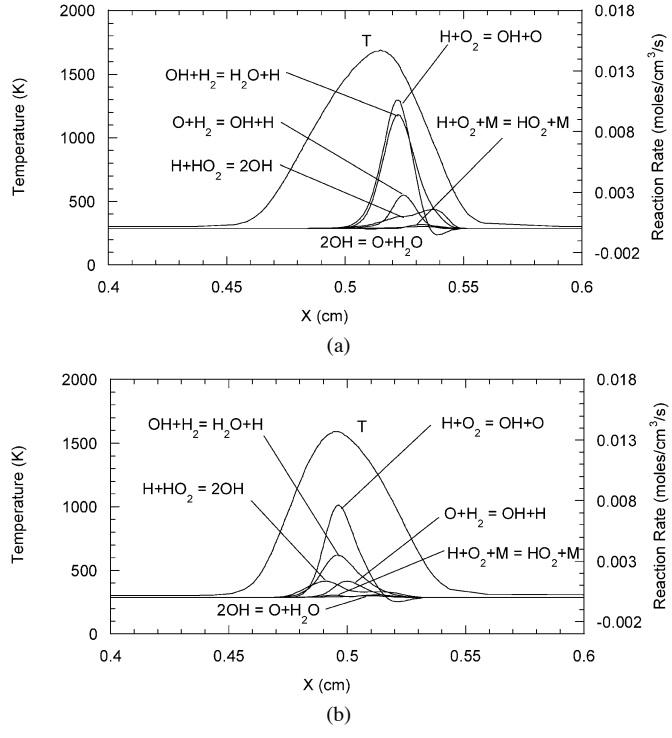

Fig. 8. Reaction rate profiles for the primary radical production reactions and temperature for C_2H_4 flames: (a) fuel/air, $Z_{st} = 0.064$ and (b) diluted fuel/oxygen-enriched air, $Z_{st} = 0.65$.

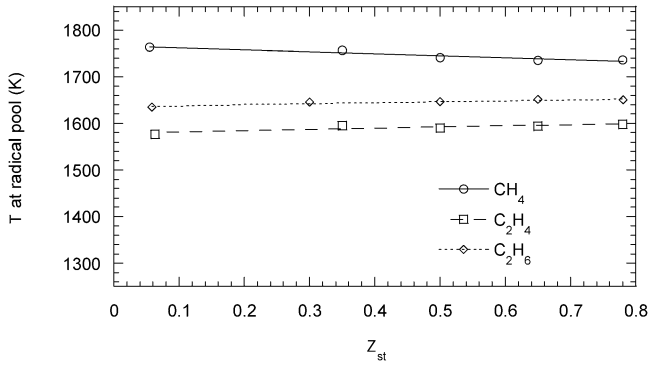

Fig. 9. Temperature at the radical production zone for all flames near extinction.

dard fuel/air flame, the location of radical production does not correspond to the location of peak temperature. The reason for this is that reaction (6) is a high activation energy reaction and thus requires both high O_2 concentration and high T. For the typical hydrocarbon/air flame the O_2 concentration falls off sufficiently far from the peak temperature that the radical production zone must lie toward the oxidizer side of the peak temperature. This displacement suggests that the *local* extinction temperature at the radical production zone—which is the critical temperature required for the radical chemistry—is much lower than the peak temperature. For CH_4 flame A, the corresponding temperature is around 1740 K as compared to a peak temperature greater than 1800 K. Comparing this temperature with the peak temperature for CH_4 flame D, one finds that they are both around 1740 K. Furthermore, the radical production zone is coincident with this peak temperature for flame D. In other words, extinction is occurring when the temperature in the radical production zone falls below about 1740 K. This explains why flame D is the stronger flame: flame D makes more "efficient" use of the peak temperature for radical production. This is the case for C_2H_4 flames as well, as shown in Fig. 8.

To verify that these conclusions are not dependent on the selected reaction mechanism, a different reaction mechanism, a 58-step C1 mechanism [14], is used for the CH_4 flames to compare the results with the GRI mechanism. The two mechanisms vary significantly, e.g., for reaction (6), the A, b, and E values are, respectively,

58-step C1 mechanism,

$$2.65 \times 10^{16},\ -0.6707,\ 17041;$$

GRI mechanism,

$$5.13 \times 10^{16},\ -0.816,\ 16507.$$

The numerical results for the CH_4 flames using the 58-step C1 mechanism are described in detail in Ref. [15]. Compared with Figs. 1, 4, and 7, the results are significantly different in terms of strain rate, scalar dissipation rate, temperature near extinction, and radical production rate. Nonetheless, the trends as to how these values vary with Z_{st} are almost the same: i.e., the primary conclusions are that: (1) there is a dramatic increase in the scalar dissipation rate with Z_{st} (as much as 40 times greater than for a fuel/air flame); (2) the location of the maximum scalar dissipation rate corresponds to that of the minimum temperature; (3) there is a displacement of the peak temperature with respect to the radical production zone for flame A; and (4) the two locations are nearly coincident for flame D.

In Fig. 9, the temperature at the location of the radical pool (as depicted by the temperature where the production rate for reaction (6) is a maximum) is compared for the CH_4, C_2H_4, and C_2H_6 flames using the GRI mechanism. For each fuel, the local temperatures at the radical production zone are almost identical, which suggests the existence of a unique *local* extinction temperature. Fig. 10 shows the difference between the peak temperature (flame temperature) and radical pool temperature and in Fig. 11 the distance between the locations of the radical pool to that of the peak temperature is shown. The negative values in Fig. 11 indicate that the location of the radical pool is closer to the oxidizer side than that of the peak temperature.

From Figs. 10 and 11, one can understand why the flame temperature at extinction changes with Z_{st}: as Z_{st} increases, the peak temperature moves from the fuel side of the radical production zone to the oxidizer side. The flame temperature at extinction changes accordingly to support the *local* extinction temperature for that fuel. At higher Z_{st} the peak temperature begins to move to the oxidizer side of the radical production zone and, once again, the extinction temperature must increase because the two zones are not coincident. This is why there is a minimum extinction temperature observed in Figs. 4 and 5. Correspond-

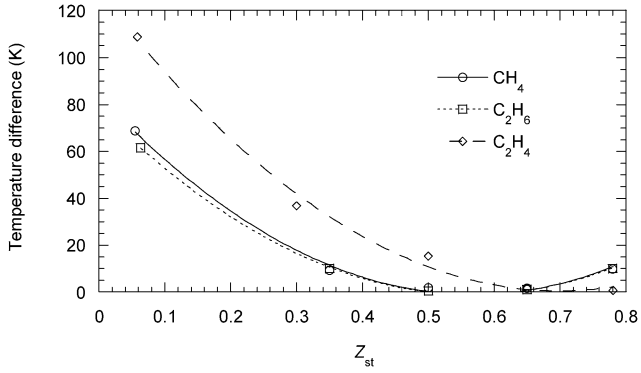

Fig. 10. Temperature difference between peak temperature and the temperature at the radical production zone for all flames near extinction.

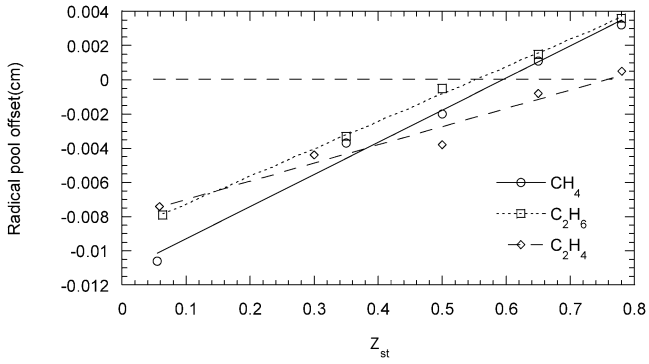

Fig. 11. The distance between the location of peak temperature and the location of the radical production zone for all flames near extinction.

ingly, χ_q decreases at higher Z_{st} because this mismatch does not allow the temperature to decrease as much before the flame extinguishes.

4. Conclusions

This work has evaluated the effects of oxygen enrichment and fuel dilution on flame extinction for a variety of fuels. As the primary goal was to evaluate the influence of flame structure on extinction, and the stoichiometric mixture fraction is a single quantity that takes into account the effects of oxygen enrichment and fuel dilution on flame structure, the results were understood in terms of stoichiometric mixture fraction. For a given fuel and a given adiabatic flame temperature, the extinction limits, as identified by the scalar dissipation rate at extinction, can vary dramatically with stoichiometric mixture fraction, even when the adiabatic flame temperature is not changed. For the fuels considered, the critical scalar dissipation rate can experience a 15- to 40-fold increase from that of neat fuel burning in air, indicating that the flame is much stronger. When the extinction scalar dissipation rate reaches a maximum, the extinction temperature reaches a minimum. This occurs when Z_{st} is around 0.5 to 0.65 (depending on the fuel), and corresponds to the condition where the radical production zone is coincident with the location of maximum temperature. This finding indicates that by adjusting the relative position of the peak temperature and the peak radical production zone (which can be done by changing Z_{st}) the extinction characteristics of the flame can be optimized.

The findings of this study indicate that oxygen enrichment, when combined with fuel dilution, can yield extremely strong flames. As oxygen-enriched combustion is growing in importance, these results can be used to optimize the mixture compositions to yield strong flames that have low emissions of soot and PAH.

Acknowledgment

This research was funded by the National Aeronautics and Space Administration with Grant NCC3-697 under the technical management of M.K. King.

References

[1] C.E. Baukal, Oxygen-Enhanced Combustion, CRC Press, Boca Raton, FL, 1998.
[2] J. Du, R.L. Axelbaum, Combust. Flame 100 (1995) 367–375.
[3] NETL Report, Carbon Sequestration: Technology Roadmap and Program Plan – 2004, April 2004.
[4] K.T. Kang, J.Y. Hwang, S.H. Chung, W. Lee, Combust. Flame 109 (1997) 266–281.
[5] S. Ishizuka, H. Tsuji, Proc. Combust. Inst. 18 (1981) 695–703.
[6] I.K. Puri, K. Seshadri, Combust. Flame 65 (1986) 137–150.
[7] C.L. Chen, S.H. Sohrab, Combust. Flame 86 (1991) 383–393.
[8] H.K. Chelliah, C.K. Law, T. Ueda, M.D. Smooke, F.A. Williams, Proc. Combust. Inst. 23 (1990) 503–511.
[9] J. Du, R.L. Axelbaum, Proc. Combust. Inst. 26 (1996) 1137–1142.
[10] N. Peters, Prog. Energy Combust. Sci. 10 (1984) 319–339.
[11] M.D. Smooke, I.K. Puri, K. Seshadri, Proc. Combust. Inst. 21 (1986) 1783–1792.
[12] A.E. Lutz, R.J. Kee, J.F. Grcar, F.M. Rupley, Oppdif—A Fortran Program for Computing Opposed-Flow Diffusion Flames, Report No. SAND96-8243, Sandia National Laboratories, 1997.
[13] G.P. Smith, D.M. Golden, M. Frenklach, N.W. Moriarty, B. Eiteneer, M. Goldenberg, C.T. Bowman, R.K. Hanson, S. Song, W.C. Gardiner Jr., V.V. Lissianski, Z. Qin, http://www.me.berkeley.edu/gri_mech/.
[14] R.W. Bilger, S.H. Starner, R.J. Kee, Combust. Flame 80 (1990) 135–149.
[15] R. Chen, Master thesis, Washington University, St. Louis (2003).